ACS Catalysis

Research Article

Cite This: ACS Catal. 2019, 9, 8810–8818

pubs.acs.org/acscatalysis

Mechanism of Organoscandium-Catalyzed Ethylene Copolymerization with Amino-Olefins: A Quantum Chemical Analysis

Jiazhen Chen,[†,§] Alessandro Motta,*[,‡,§] Jialong Zhang,[†,∥] Yanshan Gao,*[,†] and Tobin J. Marks*[,†]

[†]Department of Chemistry, Northwestern University, Evanston, Illinois 60208-3113, United States

[‡]Dipartimento di Scienze Chimiche, Università di Roma "La Sapienza" and INSTM, UdR Roma, Piazzale Aldo Moro 5, I-00185 Roma, Italy

Supporting Information

ABSTRACT: The direct, efficient copolymerization of ethylene with polar monomers represents a "holy grail" for the synthesis of polar polyethylenes; however, developing effective catalysts for such copolymerizations remains a largely unsolved challenge. Very recently, organoscandium catalysts were shown to be very active for ethylene + polar monomer [$H_2C{=}CH(CH_2)_nCH_2FG$, FG = polar functional group] copolymerization. Interestingly, comonomer enchainment selectivity decreases with increasing linker length (n), while overall polymerization activity is largely unaffected, and the intriguing mechanistic origins are not yet understood. In this study, density functional theory (DFT) methods are employed to investigate the mechanism of organoscandium-catalyzed ethylene + amino olefin (AO) copolymerization, using $(C_5Me_4SiMe_3)Sc(CH_2CH_2CH_3)^+B(C_6F_5)_4^-$ (**Sc-1**) as the model active species and *N*-(1-butenyl)^{n}Pr$_2$ and *N*-(1-octenyl)^{n}Pr$_2$ as model comonomers. Among conceivable scenarios in monomer coordination, activation, and insertion, it is found that copolymerization activity is largely governed by intermolecular amino olefin N-coordination. Amino olefin n-dependent enchainment patterns arise from chain-length regulation of the energy barrier for an amino olefin chelating "self-assisted" enchainment pathway. Short-chain *N*-(1-butenyl)^{n}Pr$_2$ enchains via a self-assisted insertion pathway (6.0 kcal/mol energy barrier), while long-chain *N*-(1-octenyl)^{n}Pr$_2$ enchains via unassisted 1,2-insertion with exogenous amine coordination (7.2 kcal/mol energy barrier). These findings explain the experimental results, showcase the characteristic reactivity of Sc catalysts in polar monomer copolymerization, and highlight the potential and challenges in developing catalysts for polar monomer copolymerization.

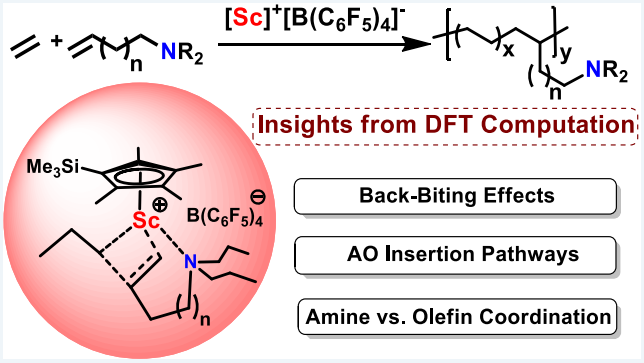

KEYWORDS: *scandium, DFT, olefin polymerization, polar monomer, amino olefin*

INTRODUCTION

Polyethylenes represent some of the most versatile and extensively manufactured polymeric materials worldwide.[1,2] Introducing polar functional groups into polyethylenes offers greatly improved chemical, physical, mechanical, and surface properties and, thus, has the potential to significantly expand polyethylene applications scope.[3,4] However, the efficient catalytic synthesis of polar polyethylenes remains a largely unsolved challenge.[5] Direct coordinative copolymerization of polar monomers with ethylene would seem to be the most atom- and energy-efficient strategy for producing polar polyethylenes.[6] For this reason the development of transition metal catalysts for efficient polar monomer copolymerization has become a central topic of intense research activity.[7]

The challenge associated with polar monomer copolymerization originates from the strong interaction between typical Lewis-acidic cationic metal catalyst centers and Lewis-basic polar functional groups (Scheme 1). To address this issue, several strategies have been employed. Less oxophilic late transition metal (Ni, Pd) catalysts are generally more tolerant of polar functionality and have demonstrated progress in tackling this challenge.[8,9] However, major limitations toward industrial application remain, including overall modest activity, a lack of control over the regio- and stereochemistry of polar monomer insertion, and low M_n due to rapid competing β-H elimination.[10,11] Group 4 catalysts have also been reported in polar monomer copolymerizations.[12−17] However, direct masking reagent-free copolymerizations are limited to certain amino olefin comonomers;[12] for most of the reported catalyst systems, large excesses of Al cocatalyst and/or sacrificial masking reagents such as trialkylaluminum (AlR_3) are often used, thus compromising the atom economy and increasing the

Received: June 3, 2019
Revised: August 13, 2019
Published: August 13, 2019

DOI: 10.1021/acscatal.9b02317
ACS Catal. 2019, 9, 8810–8818

Scheme 1. Mechanistic Scenarios for Metal-Catalyzed Copolymerization of Ethylene with a Functional Group (FG)-Containing α-Olefin; Counteranions Omitted for Clarity

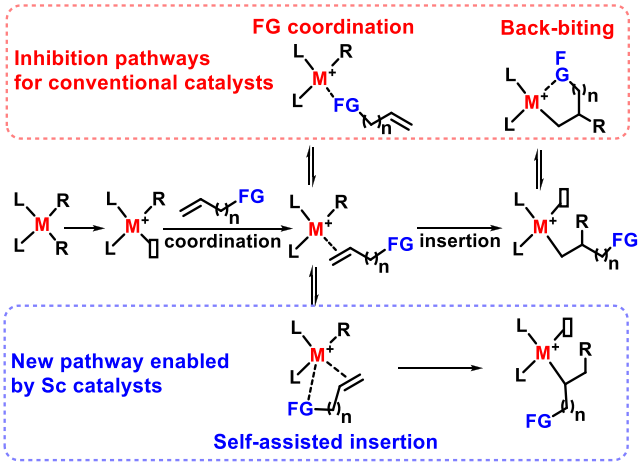

cost and complexity of the processes.[14−17] Furthermore, the comonomer scope is usually limited to comonomers with relatively long $(-CH_2)_n-$ linkers between the olefin and the polar group.[12,18]

Rare earth metal catalysts recently emerged as an intriguing and promising alternative. Their tolerance toward polar functionality has been demonstrated in Ln-catalyzed chain-transfer polymerization[19] and unprotected polar styrene polymerization.[20−25] Scandium is unique as it represents the smallest ion in the rare earth series with covalency in between group 4 metals and lanthanides.[26−28] Recently, this laboratory[29] and Hou and co-workers[30,31] reported that organoscandium complexes are active catalysts for ethylene + functionalized α-olefin copolymerization upon activation with trityl perfluoroaryl borate, $Ph_3C^+B(C_6F_5)_4^-$. Both the activity and comonomer enchainment level are remarkable. Amino olefins ($CH_2{=}CH(CH_2)_nCH_2NR_2$, AO, Scheme 2) are

Scheme 2. Catalytic Ethylene + Amino Olefin Copolymerization at a Cationic Organoscandium Center

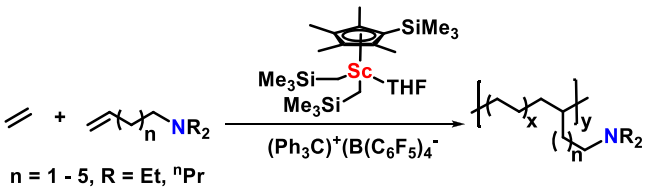

particularly attractive comonomer candidates because pendent dialkyl amino groups in polyolefins enhance their surface properties,[32] serve as a scaffold for nanoparticle catalysts,[33,34] increase polyolefin thermal stability,[35] and form ionic polymers upon additional modification.[36] In Sc-catalyzed ethylene + AO copolymerizations (Scheme 2), a positive correlation between shorter chain length (n) and higher AO incorporation levels was discovered, whereas the overall polymerization activities are not significantly correlated with AO chain length (n).[29] Such results are very different from those of previously reported group 4[12,17] and late transition metal catalysts,[32,37] suggesting a unique operating mechanism in which the functional group plays a pivotal role (Scheme 1).

A detailed mechanistic understanding of polar comonomer enchainment processes in this emerging field has therefore become imperative for further polar monomer copolymerization methodology development. Previously, DFT and/or quantum mechanics/molecular mechanics (QM/MM) studies were successfully employed to probe mechanistic details in Sc-catalyzed olefin polymerization such as the origin of regio- and stereoselectivity,[38−40] evaluation of chain initiation efficiency of various Sc-alkyl precursors,[41] and elucidation of the roles of ancillary ligand, metal, and solvation on the structure and stability of the active species.[42,43] In Sc-catalyzed functionalized monomer homopolymerization, DFT calculations have been used to understand the syndioselectivity in functionalized α-olefin homopolymerizations[30] and step growth versus chain growth pathways in functionalized styrene homopolymerizations.[44] A recent study by Cui, Maron, and co-workers highlighted the importance of Sc···phenyl interactions in regulating monomer insertion in ethylene + polar styrene copolymerizations.[20] While these studies focused on polar monomer homopolymerizations or ethylene + polar styrene copolymerizations, interesting mechanistic questions in ethylene + polar α-olefin copolymerization remain currently unaddressed. Thus, the mechanistic origins of copolymerization activity and polar monomer enchainment pattern are intriguing targets for investigation. Understanding these mechanisms will fuel and guide the development of future rare-earth catalyst systems. Here we employ DFT computation to investigate ethylene + amino olefin copolymerization mechanisms by examining the energetics of coordination, activation, and insertion pathways.

■ COMPUTATIONAL DETAILS

Calculations were performed adopting the M06 hybrid meta-GGA functional.[45] M06 considers medium-range correlation energy (e.g., medium-range dispersion forces) that can play a significant role when bimolecular steps are involved in the catalytic cycle. Moreover, the meta-hybrid functional provides a generally better performance compared to the GGA (such as PBE) and the hybrid (such as B3LYP) functionals.[46] Previous investigation of different functional types (GGA, hybrid, and meta-hybrid) for homogeneous group 3 catalysis suggests that M06 is a reliable choice.[47] The effective core potential of Hay and Wadt[48] (LANL2DZ) and the relevant basis sets were used for the scandium and silicon atoms. The standard all-electron 6-31G** basis[49] was used for all the other atoms. Molecular geometry optimization of stationary points was carried out without symmetry constraints and used analytical gradient techniques. Default values in the Gaussian 16 code were used for the geometry optimization. In particular, the Berny algorithm using GEDIIS[50] was adopted. Convergence criteria are based on a maximum force and displacement of 4.5×10^{-4} Ha/Å and 1.8×10^{-3} Å, respectively, and a relative RMS of 3.0×10^{-4} Ha/Å and 1.2×10^{-3} Å, respectively. The transition states were searched with the "distinguished reaction coordinate procedure" along the emerging C−C bonds.[51,52] This procedure starts by choosing a particular internal coordinate (distance, angle, and torsion) as the reaction coordinate and then performs an energy scan along this reaction coordinate. The goal is to determine the maximum energy value and the minimum force value along the selected internal coordinate, which should correspond to a saddle point of the potential energy surface (PES). Saddle points are then verified by the presence of only one negative frequency along

DOI: 10.1021/acscatal.9b02317
ACS Catal. 2019, 9, 8810−8818

the direction of the reaction coordinate. Frequency analysis was also performed to obtain thermochemical information about the reaction pathways at 298.15 K and 1 atm using the harmonic approximation.

Solvation effects were modeled using the polarized continuum model (PCM).[53] The PCM models the solvent as a continuum of uniform dielectric constant, and the solute is placed in a cavity within the solvent. In this case the modeled solvent is toluene (ε = 2.3741 D). A single-point energy calculation on the optimized geometries is then performed to take into account the solvent effects.[54] Moreover, the differences of translational and rotational entropy when moving from ideal gas phase to a real solvent are taken into account by adding an energy contribution of 8RT (4.74 kcal/mol at room temperature) to the Gibbs free energy of each species.[55−57] In fact, it is well-known that the Gibbs energy profile shifts upward compared to the SCF or E_{ZPE} profile when associative processes are involved, mainly due to the translational/rotational entropy loss. However, the translational/rotational entropy loss computed as an ideal gas is known to be overestimated in a solvent and the real free energy is known to lie somewhere in between the SCF and the Gibbs free energy profiles.[58,59] The correction employed here reduces the effect of the translational/rotational entropy loss evaluated for a bimolecular process at the ideal gas level to better mimic the Gibbs free energy profile in solution. This correction is important mainly when processes with different molecularity are compared. In the present case, this effect is taken into account to better compare insertion pathway C with insertion pathways A and B. The effect of concentration when moving from 1 atm to 1 M is taken into account by adding an energy contribution of 1.89 kcal/mol (RT ln(P_{1M}/P_{1atm})) to each species. All calculations were performed using the G16 code[60] on Linux cluster systems.

The counteranion was modeled exactly as the $B(C_6F_5)_4^-$ species, and the growing polymer chain was modeled by an *n*-propyl group. The *n*-propyl group was chosen because no AO−AO (amino olefin−amino olefin) diads are observed in the polymerization process. Thus, AO coordination/insertion processes follow an ethylene molecule insertion. The model active species used in these calculations is $(C_5Me_4SiMe_3)Sc(CH_2CH_2CH_3)^+B(C_6F_5)_4^-$ (**Sc-1**, Figure 1). The tetrahydrofuran (THF) coordinated to Sc in the precatalyst $(C_5Me_4SiMe_3)Sc(CH_2SiMe_3)_2(THF)$ (Scheme 2) was not included in the model structure because a previous study on the same catalyst suggests that the THF-free species is the true active catalyst during the chain propagation.[61] Two amino olefins were considered to probe linker-length (n) effects: the short-chain *N*-(1-butenyl)^{n}Pr$_2$ and the long-chain *N*-(1-octenyl)^{n}Pr$_2$. Note that the counteranion $B(C_6F_5)_4^-$ is included in all calculations described here unless otherwise noted.

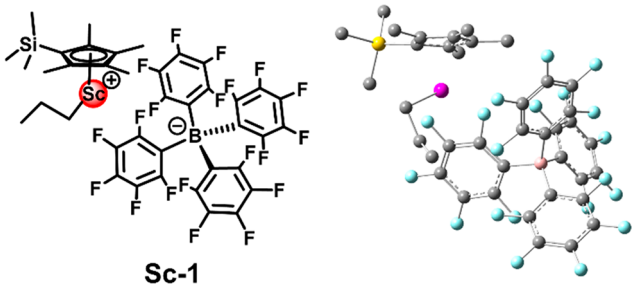

Figure 1. Model active species $(C_5Me_4SiMe_3)Sc(CH_2CH_2CH_3)^+B(C_6F_5)_4^-$ (**Sc-1**) (left) and its optimized structure (right) with H atoms omitted for clarity.

In some representative cases, a conformational analysis was conducted to obtain the most stable configurations. In particular, different arrangements of the ligands and other groups (Cp, olefin, counteranion, and growing chain) around the Sc were examined. The effect of the conformation of the growing chain as well as the effect of the conformation of the $Si(Me_3)Cp$ ligand were evaluated (see Supporting Information for details). Moreover, for a better comparison between the short- versus long-chain AO insertions, we used analogous starting geometries for both of them. For insertion pathways A and C, for example, we assumed a standard linear arrangement of the AO chain for both butenyl and octenyl cases.

RESULTS AND DISCUSSION

To understand the polymerization mechanism and differences between short-chain and long-chain amino olefins, DFT studies were carried out on key processes in ethylene + AO copolymerization including AO coordination, AO insertion, intramolecular coordination between amine (from inserted amino olefin) and Sc, and ethylene activation/insertion in the presence of AO.

Molecular Structure of the Ion Pair. It is well-documented that cation−anion pairs represent the active species in Sc-catalyzed olefin polymerizations from both experimental[62] and computational evidence.[42] In the optimized structure of the model ion pair **Sc-1**, the $B(C_6F_5)_4^-$ anion coordinates to the Sc center via interactions with the aryl *o*- and *m*-F atoms (Figure 1). This coordination manner has previously been observed in computational models[42] and in the solid-state structures[62] of similar ion pairs.

Amino Olefin Coordination/Activation. When the amino olefin approaches the cationic Sc center, there are three different coordination modes available: amine σ-coordination, olefin π-coordination, or simultaneous intramolecular coordination of both amine and olefin. For *N*-(1-butenyl)^{n}Pr$_2$ (Figure 2), the most stable configuration involves simultaneous coordination of both amine and olefin functionalities (ΔG = −11.0 kcal/mol). The contribution of both interactions can be evaluated by modeling the dissociation of either the amine coordination or the olefin coordination. The energy required to dissociate the olefin or amine coordination is 1.2 or 5.5 kcal/mol, respectively.

In contrast, in the case of *N*-(1-octenyl)^{n}Pr$_2$, the most stable configuration involves only the amine σ-coordination mode (Figure 3). Shifting from the amine σ-coordination to olefin π-coordination requires 6.1 kcal/mol. Unlike *N*-(1-butenyl)^{n}Pr$_2$, simultaneous coordination of both amine and olefin requires 9.6 kcal/mol in the case of *N*-(1-octenyl)^{n}Pr$_2$, likely reflecting the greater strain and steric interactions of the long alkyl chain compared to the short one.

Note that the $B(C_6F_5)_4^-$ counteranion coordinates to Sc in different modes in these coordination complexes. $B(C_6F_5)_4^-$ coordinates to the Sc center via *o*- and *m*-F atoms in the olefin coordinated species. However, in the amine coordinated complexes, a single *p*-F atom in $B(C_6F_5)_4^-$ coordinates to Sc. In contrast, for the simultaneous amine and olefin coordination, there are no close $B(C_6F_5)_4^-$ contacts to the cationic Sc center (see Figures S1 and S2 for metrical details).

DOI: 10.1021/acscatal.9b02317
ACS Catal. 2019, 9, 8810−8818

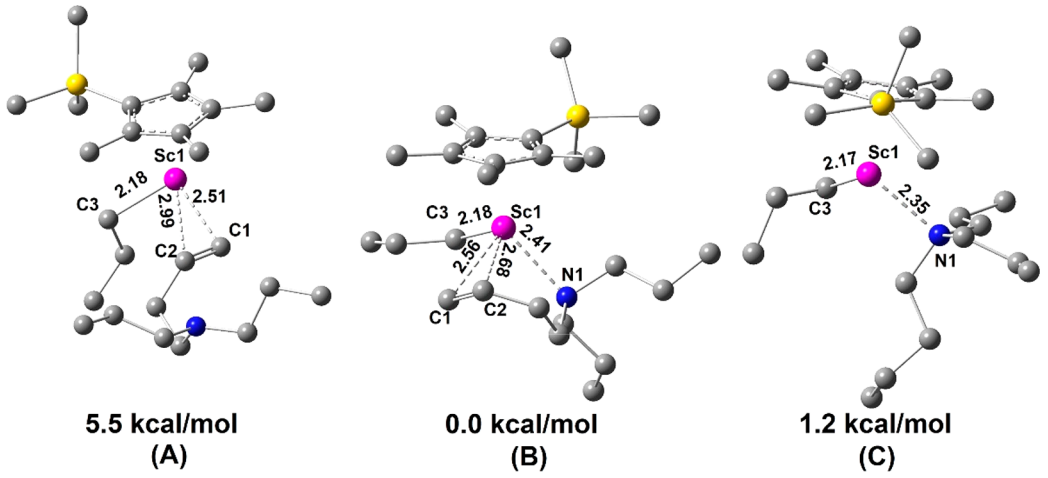

Figure 2. Cationic **Sc-1** coordination complexes with *N*-(1-butenyl)^{n}Pr$_2$ and their relative free energies. The most stable coordination complex is used as a 0.0 kcal/mol reference. Counteranion and H atoms omitted for clarity. Atom···atom distances in Å. Comonomer coordination mode: olefin-only coordination (A), simultaneous amine + olefin coordination (B), and amine-only coordination (C). For ease of visualizing the catalytic centers, the B(C$_6$F$_5$)$_4^-$counteranion is not shown.

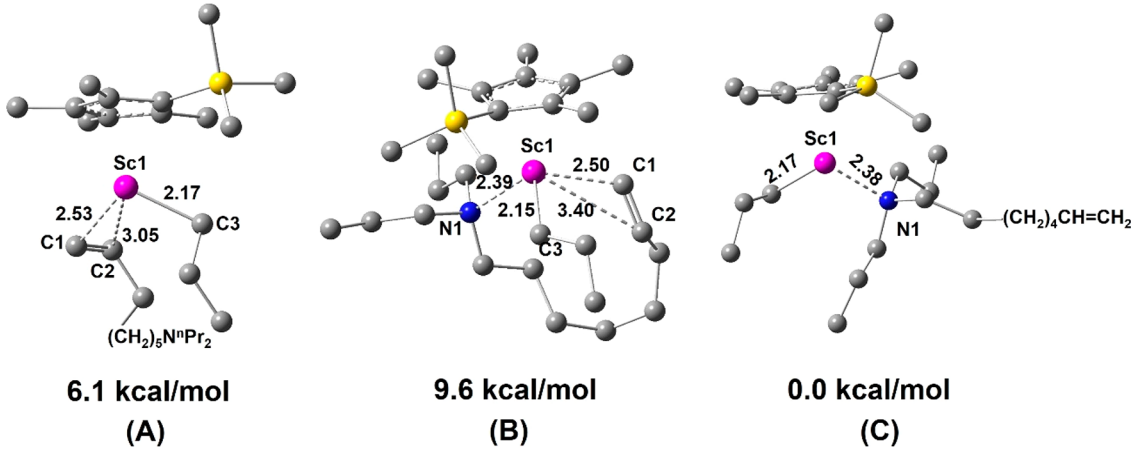

Figure 3. Cationic **Sc-1** coordination complexes with *N*-(1-octenyl)^{n}Pr$_2$ and their relative free energies. The most stable coordination complex is used as a 0.0 kcal/mol reference. Counteranion and H atoms omitted for clarity. Atom···atom distances in Å. Comonomer coordination mode: olefin-only coordination (A), simultaneous amine + olefin coordination (B), and amine-only coordination (C). For ease of visualizing the catalytic centers, the B(C$_6$F$_5$)$_4^-$counteranion is not shown.

The calculations for AO coordination suggest that *N*-(1-butenyl)^{n}Pr$_2$ adopts simultaneous olefin + amine coordination, which is likely to be favorable for subsequent intramolecular olefin activation and insertion. In contrast, *N*-(1-octenyl)^{n}Pr$_2$ adopts amine-only coordination as the energetically favored conformation, making subsequent olefin activation/insertion less favorable.

Amino Olefin Insertion Pathways. Plausible amino olefin insertion pathways are shown in Scheme 3 and Figures 4 and 5 and are categorized by olefin insertion regiochemistry, as well as whether and how the amine group is involved. Olefin undergoes 1,2- or 2,1-insertion, and olefin insertion occurs either without amine coordination (Scheme 3A), with amine coordination from the same amino olefin (amine-assisted insertion, Scheme 3B), or with amine coordination by another amino olefin molecule (unassisted insertion with amine coordination, Scheme 3C).

For *N*-(1-butenyl)^{n}Pr$_2$ with 1,2-insertion, the self-assisted pathway ($\Delta G^{\ddagger}$ = 6.0 kcal/mol) is the kinetically preferred pathway but only by a narrow margin (Table 1). The unassisted pathway in the presence of amine coordination from another amino olefin molecule lies at 1.7 kcal/mol higher in energy ($\Delta G^{\ddagger}$ = 7.7 kcal/mol, Figure 6C). In contrast, the insertion without amine coordination is not favorable in the present system, having a much higher energy barrier ($\Delta G^{\ddagger}$ = 12.9 kcal/mol, Figure 6A). Regarding olefin insertion regiochemistry, the preference between 1,2-insertion and 2,1-insertion is also analyzed. Our results suggest that 1,2-insertion ($\Delta G^{\ddagger}$ = 6.0 kcal/mol, Figure 6B) has an almost identical energy barrier compared to 2,1-insertion ($\Delta G^{\ddagger}$ = 6.1 kcal/mol) in the self-assisted enchainment pathway (Scheme 3B). For the insertion pathway without amine coordination (Scheme 3A), the 1,2-insertion is preferred over 2,1-insertion (12.9 vs 20.0 kcal/mol). A similar scenario is found for unassisted insertion with amine coordination (Scheme 3C) in which the transition state (TS) for 1,2-insertion lies 4.4 kcal/mol below that for 2,1-insertion (Table 1).

Note that Hou, Luo, and co-workers reported that 2,1-insertion is preferred in Sc-catalyzed homopolymerization of 4-phenylthio-1-butene, supported by DFT evidence.[30] The difference is likely attributable to the different model complexes used, (C$_5$Me$_4$SiMe$_3$)Sc-CH$_2$CH$_2$CH$_3^+$B(C$_6$F$_5$)$_4^-$

DOI: 10.1021/acscatal.9b02317
ACS Catal. 2019, 9, 8810−8818

Scheme 3. Possible Scenarios for Amino Olefin Insertion at a Cationic Organoscandium Center; Counteranion and $C_5Me_4SiMe_3$ Ligand Omitted for Ease of Viewing

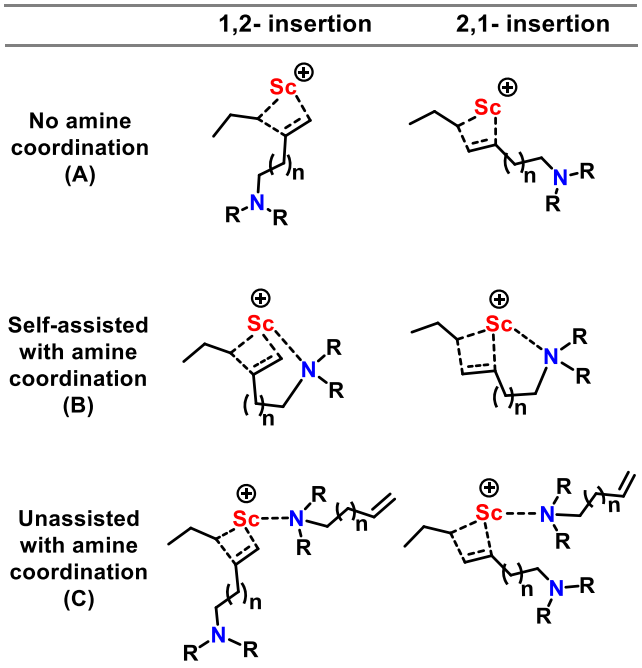

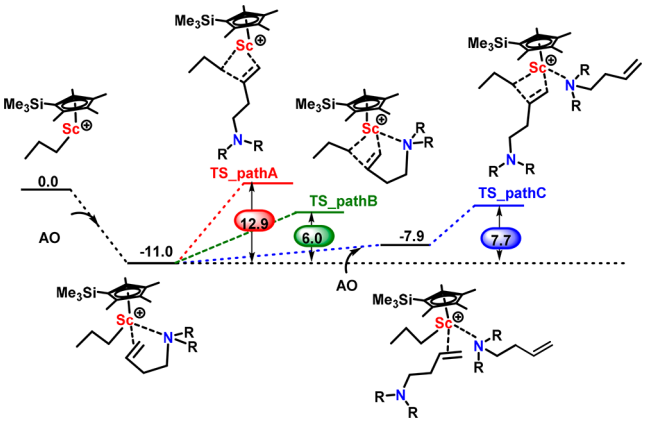

Figure 4. Gibbs free energy profiles (kcal/mol) for the *N*-(1-butenyl)^{n}Pr$_2$ incorporation (1,2-insertion) step evaluated along three pathways. Pathway A, no amine coordination; pathway B, self-assisted with amine coordination; pathway C, unassisted with amine coordination.

here versus $(C_5Me_4H)Sc\text{-}(CH_2C_6H_4NMe_2\text{-}o)^+$ in ref 30. The counteranion $B(C_6F_5)_4^-$ introduces new steric bulk, which will likely affect the TS energetic profiles in different manners for the 1,2- and 2,1-insertion pathways. Comparing the present calculation results from naked cation to the ion-pairing approach, the energy barrier for 2,1-insertion remains similar (6.9 kcal/mol for the naked cation versus 6.1 kcal/mol for the ion pair). In marked contrast, the energy barrier for the 1,2-insertion pathway clearly decreases from 9.5 kcal/mol for the naked cation to 6.0 kcal/mol for the ion pair. Therefore, the preferred insertion pathway switches from a 2,1- to 1,2-insertion when the more complete ion pair approach is employed instead of a simple naked ion. Note that 1,2- or 2,1-AO insertion cannot be distinguished from the NMR spectra

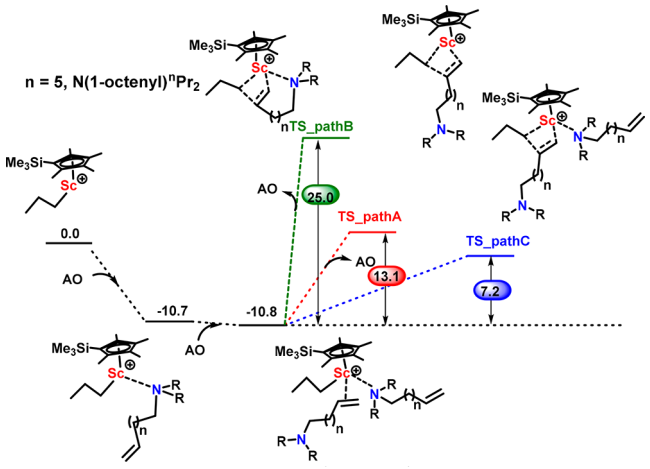

Figure 5. Gibbs free energy profiles (kcal/mol) for the long AO incorporation (1,2 insertion) step evaluated along three pathways. Pathway A, no amine coordination; pathway B, self-assisted with amine coordination; pathway C, unassisted with amine coordination.

Table 1. Energetic Barriers (kcal/mol) for 1,2- and 2,1-Insertion Pathways for *N*-(1-Butenyl)^{n}Pr$_2$ and *N*-(1-Octenyl)^{n}Pr$_2$

	no amine coordination (A)	self-assisted with amine coordination (B)	unassisted with amine coordination (C)
		N-(1-butenyl)^{n}Pr$_2$	
1,2-insertion	12.9	6.0	7.7
2,1-insertion	20.0	6.1	12.1
		N-(1-octenyl)^{n}Pr$_2$	
1,2-insertion	13.1	25.0	7.2
2,1-insertion	23.2	25.1	10.0

of ethylene + AO copolymers because no AO−AO diads are formed.[12,29]

As for the long-chain AO *N*-(1-octenyl)^{n}Pr$_2$ (Figure 5), the amine-coordinated, self-assisted pathway is significantly disfavored ($\Delta G^{\ddagger}$ = 25.0 kcal/mol versus 6.0 kcal/mol for *N*(1-butenyl)^{n}Pr$_2$) (Table 1). The increased energetic barrier mainly reflects geometrical penalties for forcing the octenyl chain to adopt an unfavored cyclic conformation that requires more distorted sp^3 carbons.[7,12,63] Chain length has a less profound but still significant effect on the other pathways, namely, insertion without amine coordination and amine-coordinated unassisted insertion pathways, because the linker between olefin and amine moieties is not directly involved in these pathways. Compared to *N*-(1-butenyl)^{n}Pr$_2$, the energetic barriers for *N*-(1-octenyl)^{n}Pr$_2$ are higher. The Gibbs free energy for *N*-(1-octenyl)^{n}Pr$_2$ 1,2-insertion without amine coordination is 13.1 versus 12.9 kcal/mol for *N*-(1-butenyl)^{n}Pr$_2$. The Gibbs free energy for *N*(1-octenyl)^{n}Pr$_2$ 1,2-insertion with amine coordination is 7.2 versus 7.7 kcal/mol for *N*-(1-butenyl)^{n}Pr$_2$ (Table 1 and Figure 5).

Taking all the enchainment pathways investigated here together, *N*-(1-butenyl)^{n}Pr$_2$ enchainment proceeds via a unique self-assisted 1,2-insertion pathway with a 6.0 kcal/mol energy barrier. In contrast, *N*-(1-octenyl)^{n}Pr$_2$ undergoes insertion via an unassisted pathway with amine coordination and has a 7.2 kcal/mol barrier. Importantly, these results are well-tuned with the experimental ethylene + AO copolymerization data revealing the more efficient insertion of short-

DOI: 10.1021/acscatal.9b02317
ACS Catal. 2019, 9, 8810−8818

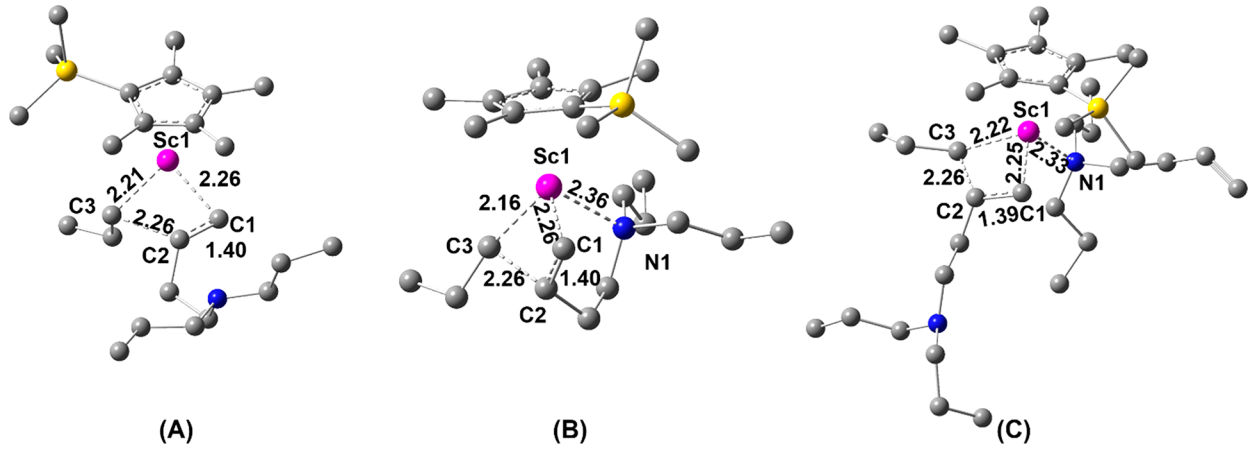

Figure 6. Structures of *N*-(1-butenyl)^{n}Pr$_2$ 1,2-insertion transition states with counteranion and H atoms omitted for ease of viewing. Atom···atom distances in Å. No amine coordination (A), self-assisted with amine coordination (B), and unassisted with exogenous amine coordination (C).

chain *N*-(1-butenyl)^{n}Pr$_2$ compared to long-chain *N*-(1-octenyl)^{n}Pr$_2$ under the same reaction conditions (2.0% versus <0.1%).[29] Note that chain-length-dependent activities were also observed in organolanthanide-mediated hydroamination/cyclization reactions, where the cyclization rate of 1-amino-pent-4-ene is 28× faster than that of 1-aminohex-5-ene.[64]

Intramolecular Amine Coordination after Amino Olefin Enchainment. After the amino olefin monomer is inserted, it may affect subsequent monomer insertion events through amine coordination. Such intramolecular Lewis basic group coordination to a metal center is also known as a "backbiting" effect, which acts as a major inhibition pathway in transition metal-catalyzed ethylene copolymerization with polar monomers.[7,9,65] Such effects are implicated by a positive correlation between longer comonomer chain length and higher polymerization activity.[7,12,18,66]

To probe potential backbiting effects in the present organoscandium catalyst system, two amino olefins, *N*-(1-butenyl)^{n}Pr$_2$ and *N*-(1-octenyl)^{n}Pr$_2$, are studied (Scheme 4). In the case of *N*-(1-butenyl)^{n}Pr$_2$, the thermodynamic driving force for amine coordination is minimal (ΔG = +4.3 kcal/mol). Insertion of the next ethylene into the catalytic center can be slightly affected by the amine coordination, and the overall polymerization activity should not be significantly suppressed by this chelating coordination. On passing to *N*-(1-octenyl)^{n}Pr$_2$, the chelation effect is further weakened due to the stronger penalty associated with the more unfavorable ring conformation required for Sc···N coordination of the octyl chain compared to the butyl chain.[12] Thus, amine coordination is strongly disfavored (ΔG = +15.5 kcal/mol).

Scheme 4. Computed Equilibria of Inserted Amine Coordination to the Indicated Sc Cationic Center; $B(C_6F_5)_4^-$ Counteranion Omitted for Ease of Viewing; ΔG in kcal/mol

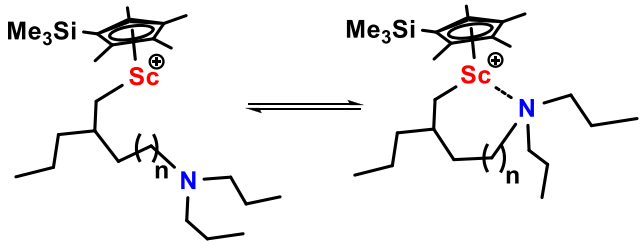

	ΔG	K
N(1-butenyl)^{n}Pr$_2$	4.3	7.0 x 10^{-4}
N(1-octenyl)^{n}Pr$_2$	15.5	4.3 x 10^{-12}

These DFT results suggest that backbiting effects are minimal regardless of the chain length, mirroring the insignificant correlation between AO linker length and polymerization activity for organoscandium-catalyzed ethylene + AO copolymerization in our previous experimental studies.[29] The computational analysis here also indicates that the major inhibition mechanism is intermolecular amine coordination[67] because intramolecular amine coordination is insignificant. This argument is supported by our experimental control experiments in which added *N*^{n}Pr$_3$ and *N*-(alkenyl)^{n}Pr$_2$ inhibit copolymerization activity to a similar extent.[29] These results are in sharp contrast to well-studied d^0 group 4 metal catalysts,[12,16] which suffer from severe backbiting poisoning effects, and highlight the potential of small rare-earth metals, especially scandium, in polar monomer copolymerization.

Ethylene Insertion in the Presence of AOs. The overall copolymerization activity is determined not only by the AO activation/insertion rate but also by the ethylene activation/insertion rate. Furthermore, the AO enchainment selectivity is determined by the relative ratio of AO insertion versus ethylene insertion. Ethylene activation/insertion is inevitably affected by the presence of AO. Ethylene stabilizes cationic Sc species to a lesser extent than *N*-(1-butenyl)^{n}Pr$_2$, −5.6 versus −11.0 kcal/mol (Figure 5), suggesting that the equilibrium shifts toward amino olefin coordination. Thus, the concentration of ethylene-coordinated species decreases in the presence of amino olefin. There are two potential ethylene insertion pathways as shown in Figure 5. Ethylene can undergo enchainment at the amine-coordinated Sc center with an energy barrier of 5.6 kcal/mol. Ethylene can also replace the AO molecule and insert at Sc without amine coordination, with a free energy barrier of 9.0 kcal/mol (Figure 7). Replacement of the AO with ethylene occurs through an associative mechanism. Both pathways have higher activation barriers than ethylene insertion in the absence of amino olefin (3.6 kcal/mol), suggesting that the presence of the AO substrate suppresses the overall polymerization activity. The energetic barrier for the self-assisted *N*-(1-butenyl)^{n}Pr$_2$

DOI: 10.1021/acscatal.9b02317
ACS Catal. 2019, 9, 8810−8818

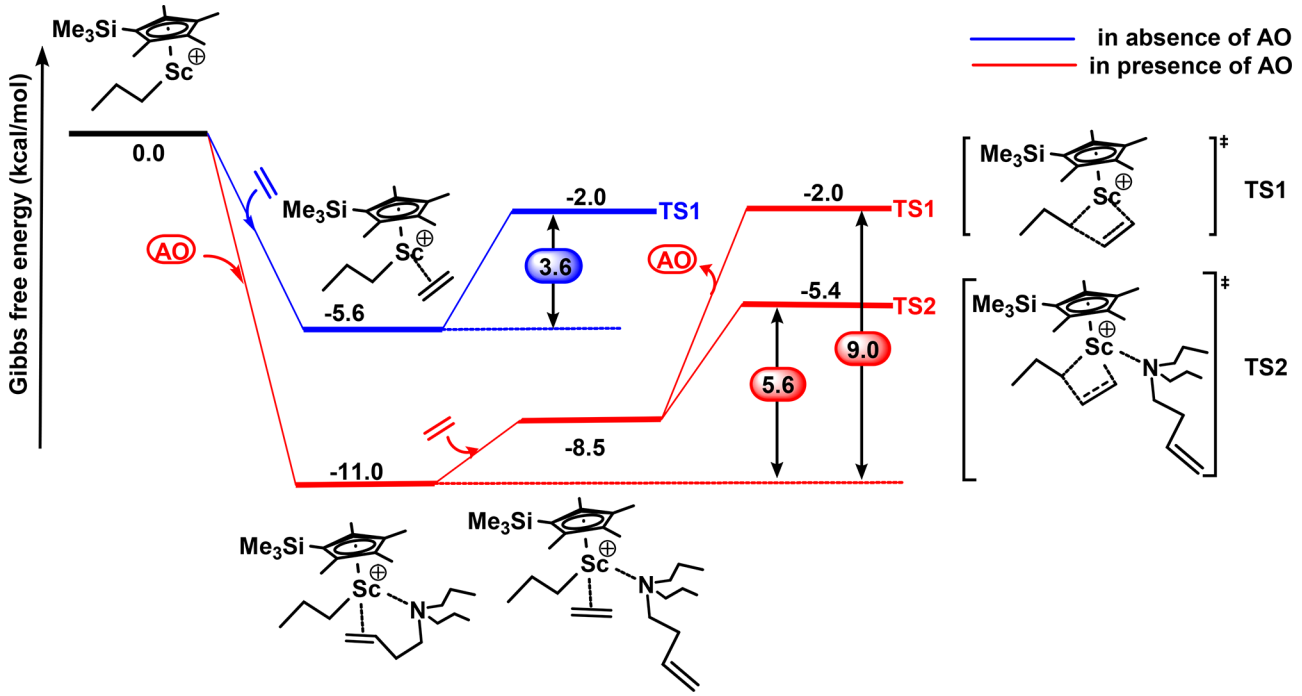

Figure 7. DFT energy profiles for ethylene insertion into **Sc-1** in the presence and the absence of the comonomer *N*-(1-butenyl)^{n}Pr$_2$.

incorporation pathway is only +0.4 kcal/mol higher than the barrier for ethylene insertion in the presence of *N*-(1-butenyl)^{n}Pr$_2$ (6.0 versus 5.6 kcal/mol) (Figure 7). Thus, significant amounts of *N*-(1-butenyl)^{n}Pr$_2$ can be incorporated in ethylene copolymerization, as observed experimentally.[29]

CONCLUSIONS

We have systematically investigated the mechanistic details of organoscandium-catalyzed ethylene copolymerization with the amino olefins *N*-(1-butenyl)^{n}Pr$_2$ and *N*-(1-octenyl)^{n}Pr$_2$ as model AOs, using DFT analysis. The major findings are summarized as follows: (i) Short-chain AOs enable simultaneous/chelating coordination of the olefin and amine moiety of the same AO, which is unavailable for long-chain AOs. (ii) Short-chain AOs insert via a chelating/self-assisted pathway, while long-chain AO insertion proceeds with a higher energetic barrier via an unassisted pathway with amine coordination from another AO. (iii) Intramolecular amine coordination after AO insertion is of minimal importance, suggesting intermolecular amine coordination is the major inhibiting factor for polymerization activity. (iv) The presence of added AO slightly increases the energetic barrier for ethylene insertion due to competing AO coordination. These DFT findings are in very good agreement with our experimental results. Linker length-dependent AO enchainment patterns are rationalized from the computed barriers for different AO insertion modes. The insignificant relationship between copolymerization activity and tertiary amine/AO identity, (1-alkenyl)N^{n}Pr$_2$ versus N^{n}Pr$_3$, is explained by evaluating amine coordination in different scenarios and their impact on copolymerization activity. Furthermore, these results highlight the advantage and potential of rare earth metals, especially scandium catalysts, for polar monomer copolymerization from a mechanistic standpoint.

ASSOCIATED CONTENT

Supporting Information

The Supporting Information is available free of charge on the ACS Publications website at DOI: 10.1021/acscatal.9b02317.

Details of conformational analysis and Cartesian coordinates of all the investigated species (PDF)

AUTHOR INFORMATION

Corresponding Authors

*E-mail: yanshan@northwestern.edu.
*E-mail: t-marks@northwestern.edu.
*E-mail: alessandro.motta@uniroma1.it.

ORCID

Jiazhen Chen: 0000-0002-9023-3072
Jialong Zhang: 0000-0002-8205-2204
Yanshan Gao: 0000-0003-0329-705X
Tobin J. Marks: 0000-0001-8771-0141

Present Address

‖Shanghai Research Institute of Petrochemical Technology, SINOPEC, 1658 Pudong Beilu, Shanghai 201208, P. R. China

Author Contributions

§J.C. and A.M. contributed equally.

Notes

The authors declare no competing financial interest.

ACKNOWLEDGMENTS

Financial support was provided by NSF through Grant nos. CHE-1464488 and CHE-1856619 (T.J.M. and J.C.). NSF Computational resources were provided by the Northwestern University Quest High Performance Computing Cluster and CINECA Award no. HP10CFRR9A 2018 under the ISCRA initiative (to A.M.).

DOI: 10.1021/acscatal.9b02317
ACS Catal. 2019, 9, 8810−8818

REFERENCES

(1) Stürzel, M.; Mihan, S.; Mülhaupt, R. From Multisite Polymerization Catalysis to Sustainable Materials and All-Polyolefin Composites. *Chem. Rev.* **2016**, *116*, 1398−1433.

(2) Gao, Y.; Chen, J.; Wang, Y.; Pickens, D.; Motta, A.; Wang, Q. J.; Chung, Y.-W.; Lohr, T. L.; Marks, T. J. Highly Branched Polyethylene Oligomers Via Single-Site Polymerization in Very Nonpolar Media. *Nat. Catal.* **2019**, *2*, 236−242.

(3) Boaen, N. K.; Hillmyer, M. A. Post-Polymerization Functionalization of Polyolefins. *Chem. Soc. Rev.* **2005**, *34*, 267−275.

(4) Chung, T. C. M. Functional Polyolefins for Energy Applications. *Macromolecules* **2013**, *46*, 6671−6698.

(5) Keyes, A.; Basbug Alhan, H. E.; Ordonez, E.; Ha, U.; Beezer, D. B.; Dau, H.; Liu, Y.-S.; Tsogtgerel, E.; Jones, G. R.; Harth, E. Olefins and Vinyl Polar Monomers: Bridging the Gap for Next Generation Materials. *Angew. Chem., Int. Ed.* **2019**, *58*, 2−24.

(6) Franssen, N. M. G.; Reek, J. N. H.; de Bruin, B. Synthesis of Functional Polyolefins: State of the Art and Remaining Challenges. *Chem. Soc. Rev.* **2013**, *42*, 5809−5832.

(7) Boffa, L. S.; Novak, B. M. Copolymerization of Polar Monomers with Olefins Using Transition-Metal Complexes. *Chem. Rev.* **2000**, *100*, 1479−1493.

(8) Carrow, B. P.; Nozaki, K. Transition-Metal-Catalyzed Functional Polyolefin Synthesis: Effecting Control through Chelating Ancillary Ligand Design and Mechanistic Insights. *Macromolecules* **2014**, *47*, 2541−2555.

(9) Nakamura, A.; Ito, S.; Nozaki, K. Coordination-Insertion Copolymerization of Fundamental Polar Monomers. *Chem. Rev.* **2009**, *109*, 5215−5244.

(10) Tan, C.; Chen, C. Emerging Palladium and Nickel Catalysts for Copolymerization of Olefins with Polar Monomers. *Angew. Chem., Int. Ed.* **2019**, *58*, 7192−7200.

(11) Chen, C. Designing Catalysts for Olefin Polymerization and Copolymerization: Beyond Electronic and Steric Tuning. *Nat. Rev. Chem.* **2018**, *2*, 6−14.

(12) Chen, J.; Motta, A.; Wang, B.; Gao, Y.; Marks, T. J. Significant Polar Comonomer Enchainment in Zirconium-Catalyzed, Masking Reagent-Free, Ethylene Copolymerizations. *Angew. Chem., Int. Ed.* **2019**, *58*, 7030−7034.

(13) Kesti, M. R.; Coates, G. W.; Waymouth, R. M. Homogeneous Ziegler-Natta Polymerization of Functionalized Monomers Catalyzed by Cationic Group IV Metallocenes. *J. Am. Chem. Soc.* **1992**, *114*, 9679−9680.

(14) Imuta, J.-i.; Kashiwa, N.; Toda, Y. Catalytic Regioselective Introduction of Allyl Alcohol into the Nonpolar Polyolefins: Development of One-Pot Synthesis of Hydroxyl-Capped Polyolefins Mediated by a New Metallocene If Catalyst. *J. Am. Chem. Soc.* **2002**, *124*, 1176−1177.

(15) Terao, H.; Ishii, S.; Mitani, M.; Tanaka, H.; Fujita, T. Ethylene/Polar Monomer Copolymerization Behavior of Bis(Phenoxyimine)Ti Complexes: Formation of Polar Monomer Copolymers. *J. Am. Chem. Soc.* **2008**, *130*, 17636−17637.

(16) Chen, Z.; Li, J.-F.; Tao, W.-J.; Sun, X.-L.; Yang, X.-H.; Tang, Y. Copolymerization of Ethylene with Functionalized Olefins by [ONX] Titanium Complexes. *Macromolecules* **2013**, *46*, 2870−2875.

(17) Yang, X.-H.; Liu, C.-R.; Wang, C.; Sun, X.-L.; Guo, Y.-H.; Wang, X.-K.; Wang, Z.; Xie, Z.; Tang, Y. [O-NS^{R}]$TiCl_3$-Catalyzed Copolymerization of Ethylene with Functionalized Olefins. *Angew. Chem., Int. Ed.* **2009**, *48*, 8099−8102.

(18) Wang, X.; Wang, Y.; Shi, X.; Liu, J.; Chen, C.; Li, Y. Syntheses of Well-Defined Functional Isotactic Polypropylenes Via Efficient Copolymerization of Propylene with ω-Halo-α-Alkenes by Post-Metallocene Hafnium Catalyst. *Macromolecules* **2014**, *47*, 552−559.

(19) Amin, S. B.; Marks, T. J. Versatile Pathways for in Situ Polyolefin Functionalization with Heteroatoms: Catalytic Chain Transfer. *Angew. Chem., Int. Ed.* **2008**, *47*, 2006−2025.

(20) Liu, B.; Qiao, K.; Fang, J.; Wang, T.; Wang, Z.; Liu, D.; Xie, Z.; Maron, L.; Cui, D. Mechanism and Effect of Polar Styrenes on Scandium-Catalyzed Copolymerization with Ethylene. *Angew. Chem., Int. Ed.* **2018**, *57*, 14896−14901.

(21) Liu, D.; Wang, M.; Wang, Z.; Wu, C.; Pan, Y.; Cui, D. Stereoselective Copolymerization of Unprotected Polar and Nonpolar Styrenes by an Yttrium Precursor: Control of Polar-Group Distribution and Mechanism. *Angew. Chem., Int. Ed.* **2017**, *56*, 2714−2719.

(22) Guo, F.; Jiao, N.; Jiang, L.; Li, Y.; Hou, Z. Scandium-Catalyzed Syndiospecific Polymerization of Halide-Substituted Styrenes and Their Copolymerization with Styrene. *Macromolecules* **2017**, *50*, 8398−8405.

(23) Liu, D.; Wang, M.; Chai, Y.; Wan, X.; Cui, D. Self-Activated Coordination Polymerization of Alkoxystyrenes by a Yttrium Precursor: Stereocontrol and Mechanism. *ACS Catal.* **2019**, *9*, 2618−2625.

(24) Liu, D.; Yao, C.; Wang, R.; Wang, M.; Wang, Z.; Wu, C.; Lin, F.; Li, S.; Wan, X.; Cui, D. Highly Isoselective Coordination Polymerization of Ortho-Methoxystyrene with beta-Diketiminato Rare-Earth-Metal Precursors. *Angew. Chem., Int. Ed.* **2015**, *54*, 5205−5209.

(25) Li, S.; Liu, D.; Wang, Z.; Cui, D. Development of Group 3 Catalysts for Alternating Copolymerization of Ethylene and Styrene Derivatives. *ACS Catal.* **2018**, *8*, 6086−6093.

(26) Fustier, M.; Le Goff, X.-F.; Lutz, M.; Slootweg, J. C.; Mezailles, N. Scandium Carbene Complexes: Synthesis of Mixed Alkyl, Amido, and Phosphido Derivatives. *Organometallics* **2015**, *34*, 63−72.

(27) Nishiura, M.; Guo, F.; Hou, Z. Half-Sandwich Rare-Earth-Catalyzed Olefin Polymerization, Carbometalation, and Hydroarylation. *Acc. Chem. Res.* **2015**, *48*, 2209−20.

(28) Liddle, S. T.; Mills, D. P.; Wooles, A. J. Early Metal Bis(Phosphorus-Stabilised)Carbene Chemistry. *Chem. Soc. Rev.* **2011**, *40*, 2164−76.

(29) Chen, J.; Gao, Y.; Wang, B.; Lohr, T. L.; Marks, T. J. Scandium-Catalyzed Self-Assisted Polar Co-Monomer Enchainment in Ethylene Polymerization. *Angew. Chem., Int. Ed.* **2017**, *56*, 15964−15968.

(30) Wang, C.; Luo, G.; Nishiura, M.; Song, G.; Yamamoto, A.; Luo, Y.; Hou, Z. Heteroatom-Assisted Olefin Polymerization by Rare-Earth Metal Catalysts. *Sci. Adv.* **2017**, *3*, e1701011.

(31) Wang, H.; Yang, Y.; Nishiura, M.; Higaki, Y.; Takahara, A.; Hou, Z. Synthesis of Self-Healing Polymers by Scandium-Catalyzed Copolymerization of Ethylene and Anisylpropylenes. *J. Am. Chem. Soc.* **2019**, *141*, 3249−3257.

(32) Na, Y.; Zhang, D.; Chen, C. Modulating Polyolefin Properties through the Incorporation of Nitrogen-Containing Polar Monomers. *Polym. Chem.* **2017**, *8*, 2405−2409.

(33) Shi, Z.; Guo, F.; Li, Y.; Hou, Z. Synthesis of Amino-Containing Syndiotactic Polystyrene as Efficient Polymer Support for Palladium Nanoparticles. *J. Polym. Sci., Part A: Polym. Chem.* **2015**, *53*, 5−9.

(34) Xu, J.; Chen, G.; Yan, R.; Wang, D.; Zhang, M.; Zhang, W.; Sun, P. One-Stage Synthesis of Cagelike Porous Polymeric Microspheres and Application as Catalyst Scaffold of Pd Nanoparticles. *Macromolecules* **2011**, *44*, 3730−3738.

(35) Stehling, U. M.; Stein, K. M.; Fischer, D.; Waymouth, R. M. Metallocene/Borate-Catalyzed Copolymerization of 5-N,N-Diisopropylamino-1-Pentene with 1-Hexene or 4-Methyl-1-Pentene. *Macromolecules* **1999**, *32*, 14−20.

(36) Zhang, M.; Yuan, X.; Wang, L.; Chung, T. C. M.; Huang, T.; de Groot, W. Synthesis and Characterization of Well-Controlled Isotactic Polypropylene Ionomers Containing Ammonium Ion Groups. *Macromolecules* **2014**, *47*, 571−581.

(37) Radlauer, M. R.; Buckley, A. K.; Henling, L. M.; Agapie, T. Bimetallic Coordination Insertion Polymerization of Unprotected Polar Monomers: Copolymerization of Amino Olefins and Ethylene by Dinickel Bisphenoxyiminato Catalysts. *J. Am. Chem. Soc.* **2013**, *135*, 3784−3787.

(38) Luo, Y.; Luo, Y.; Qu, J.; Hou, Z. QM/MM Studies on Scandium-Catalyzed Syndiospecific Copolymerization of Styrene and Ethylene. *Organometallics* **2011**, *30*, 2908−2919.

DOI: 10.1021/acscatal.9b02317
ACS Catal. 2019, 9, 8810−8818

(39) Perrin, L.; Bonnet, F.; Visseaux, M.; Maron, L. A DFT Study of Conjugated Dienes Polymerisation Catalyzed by $[Cp^*ScR]^+$: Insights into the Propensity for Cis-1,4 Insertion. *Chem. Commun.* **2010**, *46*, 2965−2967.
(40) Li, X.; Nishiura, M.; Hu, L.; Mori, K.; Hou, Z. Alternating and Random Copolymerization of Isoprene and Ethylene Catalyzed by Cationic Half-Sandwich Scandium Alkyls. *J. Am. Chem. Soc.* **2009**, *131*, 13870−13882.
(41) Kang, X.; Zhou, G.; Wang, X.; Qu, J.; Hou, Z.; Luo, Y. Alkyl Effects on the Chain Initiation Efficiency of Olefin Polymerization by Cationic Half-Sandwich Scandium Catalysts: A DFT Study. *Organometallics* **2016**, *35*, 913−920.
(42) Wang, X.; Zhou, G.; Liu, B.; Luo, Y. Effects of Ligand, Metal, and Solvation on the Structure and Stability of Contact Ion Pairs Relevant to Olefin Polymerization Catalyzed by Rare-Earth-Metal Complexes: A DFT Study. *Organometallics* **2018**, *37*, 882−890.
(43) Wang, X.; Lin, F.; Qu, J.; Hou, Z.; Luo, Y. Dft Studies on Styrene Polymerization Catalyzed by Cationic Rare-Earth-Metal Complexes: Origin of Ligand-Dependent Activities. *Organometallics* **2016**, *35*, 3205−3214.
(44) Zhao, Y.; Luo, G.; Wang, X.; Kang, X.; Cui, D.; Hou, Z.; Luo, Y. Dft Studies on the Polymerization of Functionalized Styrenes Catalyzed by Rare-Earth-Metal Complexes: Factors Affecting C-H Activation Relevant to Step-Growth Polymerization. *Organometallics* **2018**, *37*, 3210−3218.
(45) Zhao, Y.; Truhlar, D. G. The M06 Suite of Density Functionals for Main Group Thermochemistry, Thermochemical Kinetics, Noncovalent Interactions, Excited States, and Transition Elements: Two New Functionals and Systematic Testing of Four M06-Class Functionals and 12 Other Functionals. *Theor. Chem. Acc.* **2008**, *120*, 215−241.
(46) Mardirossian, N.; Head-Gordon, M. Thirty Years of Density Functional Theory in Computational Chemistry: An Overview and Extensive Assessment of 200 Density Functionals. *Mol. Phys.* **2017**, *115*, 2315−2372.
(47) Dudnik, A. S.; Weidner, V. L.; Motta, A.; Delferro, M.; Marks, T. J. Atom-Efficient Regioselective 1,2-Dearomatization of Functionalized Pyridines by an Earth-Abundant Organolanthanide Catalyst. *Nat. Chem.* **2014**, *6*, 1100−1107.
(48) Hay, P. J.; Wadt, W. R. Ab Initio Effective Core Potentials for Molecular Calculations. Potentials for Potassium to Gold Including the Outermost Core Orbitals. *J. Chem. Phys.* **1985**, *82*, 299−310.
(49) Rassolov, V. A.; Pople, J. A.; Ratner, M. A.; Windus, T. L. 6-31g* Basis Set for Atoms K through Zn. *J. Chem. Phys.* **1998**, *109*, 1223−1229.
(50) Li, X.; Frisch, M. J. Energy-Represented Direct Inversion in the Iterative Subspace within a Hybrid Geometry Optimization Method. *J. Chem. Theory Comput.* **2006**, *2*, 835−839.
(51) Rothman, M. J.; Lohr, L. L., Jr. Analysis of an Energy Minimization Method for Locating Transition States on Potential Energy Hypersurfaces. *Chem. Phys. Lett.* **1980**, *70*, 405−9.
(52) *New Methods in Computational Quantum Mechanics Prigogine and Rice*; Wiley & Sons: 1996; p 403.
(53) Tomasi, J.; Mennucci, B.; Cammi, R. Quantum Mechanical Continuum Solvation Models. *Chem. Rev.* **2005**, *105*, 2999−3093.
(54) Caporaso, L.; Gracia-Budria, J.; Cavallo, L. Stereospecificity in Metallocene Catalyzed Acrylate Polymerizations: The Chiral Orientation of the Growing Chain Selects Its Own Chain End Enantioface. *J. Am. Chem. Soc.* **2006**, *128*, 16649−16654.
(55) Yu, Y. B.; Privalov, P. L.; Hodges, R. S. Contribution of Translational and Rotational Motions to Molecular Association in Aqueous Solution. *Biophys. J.* **2001**, *81*, 1632−1642.
(56) Wilhelm, E.; Battino, R. Thermodynamic Functions of the Solubilities of Gases in Liquids at 25.Deg. *Chem. Rev.* **1973**, *73*, 1−10.
(57) Falivene, L.; Barone, V.; Talarico, G. Unraveling the Role of Entropy in Tuning Unimolecular Vs. Bimolecular Reaction Rates: The Case of Olefin Polymerization Catalyzed by Transition Metals. *Mol. Catal.* **2018**, *452*, 138−144.
(58) Kozuch, S.; Lee, S. E.; Shaik, S. Theoretical Analysis of the Catalytic Cycle of a Nickel Cross-Coupling Process: Application of the Energetic Span Model. *Organometallics* **2009**, *28*, 1303−1308.
(59) Ardura, D.; Lopez, R.; Sordo, T. L. Relative Gibbs Energies in Solution through Continuum Models: Effect of the Loss of Translational Degrees of Freedom in Bimolecular Reactions on Gibbs Energy Barriers. *J. Phys. Chem. B* **2005**, *109*, 23618−23623.
(60) Frisch, M. J.; Trucks, G. W.; Schlegel, H. B.; Scuseria, G. E.; Robb, M. A.; Cheeseman, J. R.; Scalmani, G.; Barone, V.; Petersson, G. A.; Nakatsuji, H.; Li, X.; Caricato, M.; Marenich, A. V.; Bloino, J.; Janesko, B. G.; Gomperts, R.; Mennucci, B.; Hratchian, H. P.; Ortiz, J. V.; Izmaylov, A. F.; Sonnenberg, J. L.; Williams-Young, D.; Ding, F.; Lipparini, F.; Egidi, F.; Goings, J.; Peng, B.; Petrone, A.; Henderson, T.; Ranasinghe, D.; Zakrzewski, V. G.; Gao, J.; Rega, N.; Zheng, G.; Liang, W.; Hada, M.; Ehara, M.; Toyota, K.; Fukuda, R.; Hasegawa, J.; Ishida, M.; Nakajima, T.; Honda, Y.; Kitao, O.; Nakai, H.; Vreven, T.; Throssell, K.; Montgomery, J. A., Jr.; Peralta, J. E.; Ogliaro, F.; Bearpark, M. J.; Heyd, J. J.; Brothers, E. N.; Kudin, K. N.; Staroverov, V. N.; Keith, T. A.; Kobayashi, R.; Normand, J.; Raghavachari, K.; Rendell, A. P.; Burant, J. C.; Iyengar, S. S.; Tomasi, J.; Cossi, M.; Millam, J. M.; Klene, M.; Adamo, C.; Cammi, R.; Ochterski, J. W.; Martin, R. L.; Morokuma, K.; Farkas, O.; Foresman, J. B.; Fox, D. J. *Gaussian 16, Revision B.01*; Gaussian, Inc.: Wallingford, CT, 2016.
(61) Kang, X.; Yamamoto, A.; Nishiura, M.; Luo, Y.; Hou, Z. Computational Analyses of the Effect of Lewis Bases on Styrene Polymerization Catalyzed by Cationic Scandium Half-Sandwich Complexes. *Organometallics* **2015**, *34*, 5540−5548.
(62) Li, X.; Nishiura, M.; Mori, K.; Mashiko, T.; Hou, Z. Cationic Scandium Aminobenzyl Complexes. Synthesis, Structure and Unprecedented Catalysis of Copolymerization of 1-Hexene and Dicyclopentadiene. *Chem. Commun.* **2007**, 4137−4139.
(63) Myers, R. T. Thermodynamics of Chelation. *Inorg. Chem.* **1978**, *17*, 952−958.
(64) Gagne, M. R.; Stern, C. L.; Marks, T. J. Organolanthanide-Catalyzed Hydroamination. A Kinetic, Mechanistic, and Diastereoselectivity Study of the Cyclization of N-Unprotected Amino Olefins. *J. Am. Chem. Soc.* **1992**, *114*, 275−294.
(65) Chen, E. Y. X. Coordination Polymerization of Polar Vinyl Monomers by Single-Site Metal Catalysts. *Chem. Rev.* **2009**, *109*, 5157−5214.
(66) Wang, X.-Y.; Long, Y.-Y.; Wang, Y.-X.; Li, Y.-S. Insights into Propylene/ω-Halo-α-Alkenes Copolymerization Promoted by rac-Et(Ind)$_2$ZrCl$_2$ and (Pyridyl-Amido)Hafnium Catalysts. *J. Polym. Sci., Part A: Polym. Chem.* **2014**, *52*, 3421−3428.
(67) For detailed investigations, see section titled Ethylene Insertion in the Presence of AOs.

DOI: 10.1021/acscatal.9b02317
ACS Catal. 2019, 9, 8810−8818